

Mechanical load initiates hypertrophic scar formation through decreased cellular apoptosis

Shahram Aarabi,^{*,1} Kirit A. Bhatt,^{*,1} Yubin Shi,^{*} Josemaria Paterno,^{*} Edward I. Chang,^{*} Shang A. Loh,^{*} Jeffrey W. Holmes,[†] Michael T. Longaker,^{*} Herman Yee,[‡] and Geoffrey C. Gurtner^{*,2}

^{*}Department of Surgery, Stanford University School of Medicine, Stanford, California, USA; and

[†]Department of Biomedical Engineering, Columbia University, and [‡]Department of Pathology, New York University School of Medicine, New York, New York, USA.

ABSTRACT Hypertrophic scars occur following cutaneous wounding and result in severe functional and esthetic defects. The pathophysiology of this process remains unknown. Here, we demonstrate for the first time that mechanical stress applied to a healing wound is sufficient to produce hypertrophic scars in mice. The resulting scars are histopathologically identical to human hypertrophic scars and persist for more than six months following a brief (one-week) period of augmented mechanical stress during the proliferative phase of wound healing. Resulting scars are structurally identical to human hypertrophic scars and showed dramatic increases in volume (20-fold) and cellular density (20-fold). The increased cellularity is accompanied by a four-fold decrease in cellular apoptosis and increased activation of the prosurvival marker Akt. To clarify the importance of apoptosis in hypertrophic scar formation, we examine the effects of mechanical loading on cutaneous wounds of animals with altered pathways of cellular apoptosis. In p53-null mice, with down-regulated cellular apoptosis, we observe significantly greater scar hypertrophy and cellular density. Conversely, scar hypertrophy and cellular density are significantly reduced in proapoptotic *BclII*-null mice. We conclude that mechanical loading early in the proliferative phase of wound healing produces hypertrophic scars by inhibiting cellular apoptosis through an Akt-dependent mechanism.—Aarabi, S., Bhatt, K. A., Shi, Y., Paterno, J., Chang, E. I., Loh, S. A., Holmes, J. W., Longaker, M. T., Yee, H., Gurtner, G. C. Mechanical load initiates hypertrophic scar formation through decreased cellular apoptosis. *FASEB J.* 21, 3250–3261 (2007)

Key Words: hypertrophic scar • wound healing • fibrosis • scarring

THE IDEAL RESULT of human wounding is functional and scarless healing (1). This rarely occurs, and each year millions of trauma and burn injuries give rise to hypertrophic scars with resulting disfigurement and dysfunction (2, 3). Human hypertrophic scars can occur following any break in cutaneous integrity and

lead to contractures, erosion of skeletal structure, and lifelong disability (4, 5). The lack of insight into the mechanism of this fibroproliferative disease has impeded progress and resulted in high recurrence rates using current treatments (6). Understanding the pathophysiology of hypertrophic scarring is critical for developing effective therapeutics for this disease, as well as for other fibrotic disorders.

Potential etiologies thought to underlie human hypertrophic scar formation include mechanical loading, inflammation, bacterial colonization, and foreign-body reaction (7). Unfortunately, insight into the pathophysiology of hypertrophic scar formation has been hindered by the absence of a reliable animal model (8). However, the primary importance of mechanical loading has been suggested by a wealth of clinical observations in humans. Surgeons have known for centuries that placing a healing wound under tension results in scar hypertrophy (3). Similarly, most surgical techniques to treat hypertrophic scars reorient the direction of the wound into the direction of minimal mechanical loading (7, 9–15). Pressure therapy, one commonly used treatment for scar hypertrophy, may act by reducing the mechanical tension on healing tissue (7, 16, 17). Finally, wound environments with decreased intrinsic tension such as those present in the fetal or aged skin result in less scarring.

At the cellular level, living tissues sense alterations in mechanical forces and convert these changes into biochemical signals (18, 19). *In vitro*, extracellular forces are transduced via integrin-matrix interactions (20), which then signal to focal adhesion kinases (FAK) (21). Subsequent downstream signal propagation leads to a wide variety of cellular responses, including promotion of cell survival (22). Similar mechanotransduction events, although poorly understood, have been suggested in a range of pathological conditions, including cardiac hypertrophy (23), glomerulosclerosis (24), and pulmonary hypertension (25). However, the im-

¹ These authors contributed equally to this work.

² Correspondence: Stanford University, PSRL, GK-210, 257 Campus Dr., Stanford, CA 94305-5148, ggurtner@stanford.edu
doi: 10.1096/fj.07-8218com

portance of mechanical signal transduction in cutaneous tissue repair and regeneration has been suggested (26–28) but is still not understood *in vivo*.

Normal wound healing requires the orchestrated recruitment and expansion of different cells in healing wounds followed by their rapid disappearance. This process occurs during transition from the proliferative phase of wound healing to the remodeling phase, approximately 1 to 2 weeks following injury (29). Apoptosis is believed to play an important role in this process. While the upstream regulators of apoptosis in the wound environment remain unclear, there is evidence that Akt mediates this process (30, 31).

In this manuscript, we specifically examine the effect of mechanical loading on the processes by which cells are recruited, proliferate, and undergo programmed cell death in the wound environment. To do this, we have developed a novel murine model of hypertrophic scarring, which reproduces all of the features of human hypertrophic scarring by augmenting the mechanical stresses on murine wounds to achieve levels normally experienced by human wounds. Using this approach, we demonstrate that mechanical loading prevents apoptosis in the proliferative wound environment by activating the Akt pathway. This leads to a significant accumulation of cells and matrix and results in murine wounds that are histologically identical to human hypertrophic scars. The presence of a narrow temporal window for induction of this effect suggests a critical period where therapeutic intervention could result in a dramatic improvement of this disease in humans.

MATERIALS AND METHODS

In vivo loading

Four-week-old C57/BL6 mice were housed under standard conditions, using protocols approved by the New York University Animal Care and Use Committee. p53^{-/-} (B6129S2-Trp53^{tm1Tyj}/J) and *BclII*^{-/-} (B6129S2-*BclII*^{tm1Sjk}/J) (Jackson Laboratory, Bar Harbor, ME) were used for the knockout studies. Biomechanical loading devices were constructed from 22-mm expansion screws (Great Lakes Orthodontic Products, Tonawanda, NY) and Luhr plate supports (Stryker-Leibinger Co, Freiburg, Germany). The expansion screw was secured to the Luhr plate supports by plastic interfaces using clear epoxy (Devcon Scientific, Riviera Beach, FL) and allowed to dry overnight. This design allowed the loading device to be placed over the scars without actually contacting the wounds themselves. Two 2 cm linear full-thickness incisions (1.25 cm apart) were made on the dorsum of the mouse and then reapproximated with 6–0 nylon sutures. On postincision day 4, the sutures were removed from the scars, and two loading devices were carefully secured with 6–0 nylon sutures. One wound served as an internal control, with the device not activated, while the second wound was loaded every other day.

Prior to applying tension, two points were identified on either side of the scars using a permanent marking pen. Tension on the wounds was created by carefully distracting the expansion screws by 2 mm on postincision day 4 and 4 mm every other day thereafter. During the periods between

distractions, stress relaxation was observed due to the natural elongation of skin resulting in a continuous decrease in the force acting on the wounds. To compensate, tension was reapplied every other day for up to 2 wk. Scar tissue was harvested at 0, 1, 2, 3, 4, 6, 10, and 24 wk following initiation of strain (Supplemental Fig. 1).

At the designated time points, the mice were sacrificed, and the tissues were fixed in 10% formalin or embedded in OCT embedding compound and snap frozen in liquid nitrogen for immunohistochemistry, or preserved in TriReagent (Sigma-Aldrich, St. Louis, MO) for RNA analysis. Human hypertrophic scar tissue was obtained from the New York University (NYU) Department of Pathology and processed for routine H-E, using protocols approved by the NYU Institutional Review Board.

Biomechanical analysis

Adult and fetal murine skin specimens were obtained after euthanasia in accordance with Institutional Animal Care and Use Committee guidelines. Human specimens were obtained with full Institutional Review Board compliance from patients undergoing elective procedures. The mounted samples were tested using the Instron Mini 44 microtensometer (Instron Co., Grove City, PA). Mounted sample dimensions and the speed of distraction were kept constant while the force (N) and strain (change in unit length/original length×Young's modulus) were derived from these data.

Immunoblot

After protein standardization, 50 µg of protein was run on a 12.5% polyacrylamide gel. Protein was then transferred to a nitrocellulose membrane (Hybond-ECL; Amersham Biosciences, Piscataway, NJ) at 100 V for 90 min and blocked 1 h using 5% BSA in TBS. The samples were then subjected to immunodetection with anti-Phospho-Akt (Ser-473 and antitotal Akt Antibodies (Cell Signaling Technology, Beverly, MA) followed by donkey anti-Rabbit IgG (NA934; Amersham Biosciences). Detection was completed with ECL Plus detection reagent (RPN2132; Amersham Biosciences) and BioMax chemiluminescence film.

Histology

Routine H-E and picosirius red staining to enhance polarization of collagen fibers was performed on 5-µm-thick paraffin-embedded sections. The differences in the architecture of the experimental *vs.* the control scars were assessed using a polarizing microscope (Olympus BX51, New York, NY).

Immunohistochemistry

Standard light microscopy immunohistochemistry using the immunoperoxidase staining technique was performed on 4-µm-thick paraffin-embedded tissue sections. The sections were dewaxed, and endogenous peroxidase activity was quenched with 3% hydrogen peroxide for 10 min, followed by blocking serum for 1 h. The primary antibodies used included Cleaved Caspase-3 (Asp175) Antibody (1:200, Cell Signaling 9661), BRDU (1:100, Zymed 18–0103), CD31 (1:100, Molecular Probes, Eugene, OR), CD117 (1:200, A4502; DakoCytomation, Copenhagen, Denmark), PCNA (1:2000, SC-56; Santa Cruz Biotechnology, Santa Cruz, CA). The tissue sections were incubated with the primary antibody diluted in the blocking serum overnight at 4°C. After thorough washing with PBS, the sections were incubated with the secondary

antibody for 30 min at room temperature. This was followed by incubation with the ABC (Vectastain elite ABC kit, Vector Laboratories, Burlingame, CA) complex for 30 min at room temperature. Sections were thoroughly washed with PBS after each step. The sections were then incubated in 0.05% diaminobenzidine (DAB) until the brown substrate was formed, rinsed in distilled water, counterstained with hematoxylin (Vector), dehydrated, and mounted in VectaMount (Vector). BRDU (Zymed) staining was performed according to the manufacturer's protocol. Briefly, mice were subjected to intraperitoneal injection of 5-bromo-2'-deoxyuridine, 100 μ l, 15 mg/ml 0.9% NaCl, 60 min prior to sacrifice. Tissue sections were immunostained with anti-BrdU antibody, counterstained, and mounted.

As negative controls for the staining procedure, sections were incubated with the blocking serum only, omitting the primary antibody; the rest of the protocol was unchanged. Nonspecific brown cellular staining was not observed in any of the sections used as negative controls for the immunohistochemistry. Total cellularity was counted based on total cell counts. All histological measurements were independently determined by two blinded observers.

Morphometry

Total scar areas were evaluated on digital images (Olympus BX51) of hematoxylin-eosin stained sections, using SigmaScan image analysis software (Aspire Software International, Leesburg, VA) at $\times 100$ objective, unless otherwise noted. The images were evaluated blindly by two independent observers, and no difference was found in their data. The results are presented as means \pm SD.

Statistical analysis

The animal studies involved 3–6 mice for each treatment group. Data were analyzed using SigmaStat 2.0 (Aspire Software International, Leesburg, VA). Statistical analysis was carried out using two-tailed Student's unpaired *t* test or an analysis of variance (ANOVA). All data are presented as mean \pm SEM. Probability values of $P < 0.05$ were considered significant.

RESULTS

Differences in biomechanical properties of human and mouse skin may underlie scarring phenotypes

It is well known that adult human wounds demonstrate excessive dermal scarring, while fetal human wounds and murine wounds under normal circumstances do not (32, 33). Qualitatively, adult human skin is robustly elastic while adult murine skin has less recoil, and fetal murine skin is almost completely relaxed. To quantify these differences, we examined dynamic resting tension, a measure of the natural elasticity in these three skin types (12). Dynamic resting tension was greatest in human skin (0.132 N/mm²), followed by adult mouse skin (0.058 N/mm²), and finally fetal skin (below the limits of detection) (Fig. 1A). To further quantify the material properties of these three different skin types, we determined Young's modulus (defined as the ratio of stress over strain), a well-established measure of stiffness. Stiffness is dependent on both the resting

tension and extracellular matrix composition and is reflected in the value of the Young's modulus. Stiff materials have a high Young's modulus, and the deformation (strain) resulting from the applied force (stress) is low. On the other hand, flexible materials have a low modulus, and undergo large deformations with relatively little applied force. Again, we found that Young's modulus was greatest in human skin, followed by murine and fetal skin (Fig. 1B).

The correlation between biomechanical properties of skin and scar phenotypes (human scarring > mouse scarring > fetal scarring) suggested that inherent mechanical properties of skin might be responsible for the different healing patterns. The relatively low resting tension of murine skin also suggested that the intrinsic forces in murine skin might not be sufficient to activate the processes that lead to human hypertrophic scarring. This, in addition to extensive clinical evidence (3, 7, 10), served as the rationale for using an external tension device to augment the biomechanical forces on murine skin and replicate the forces normally experienced by human skin in a murine model.

Human levels of mechanical stress can be achieved using a novel biomechanical loading device

We constructed a novel device (Fig. 1C; see Methods) to apply tensile force to murine wounds (Fig. 1D). Intact human skin experiences 0.4–0.98 N of force at rest while healing human wounds experience 0.6 to 2 N of force (34). To duplicate these forces, we analyzed the forces present on murine skin after a standardized amount of deformation. Using regression analysis of the curves in Fig. 1B, we found that the calculated stress (Stress = 0.0013 \times (Strain²) + 0.1241 \times (Strain)) applied to murine wounds by our device was 1.5 N/mm² at day 4 and 2.7 N/mm² everyday thereafter, replicating the stresses experienced by healing human wounds. This range of stresses (1.5–2.7 N/mm²) was significantly lower than the breaking limits (9.6 N/mm²) of the murine wounds (data not shown). This protocol is depicted chronologically in Supplemental Fig. 1 (see Methods for details).

Time-dependent mechanical loading of murine wounds results in hypertrophic scar formation

By applying human levels of stress to a healing murine wound, we observed changes in scar morphology as early as 10 days after wounding. The timing of applied load was critical for the formation of hypertrophic scars. Loading during the earliest inflammatory phase (days 1–3) resulted in wound dehiscence, whereas loading during the proliferative phase of wound healing (day 3–6) resulted in hypertrophic scars. Loading later, during the remodeling phase (after day 6), had no effect on scar formation. In addition, at least 7 consecutive days of loading were required to give rise to hypertrophic scar formation (data not shown).

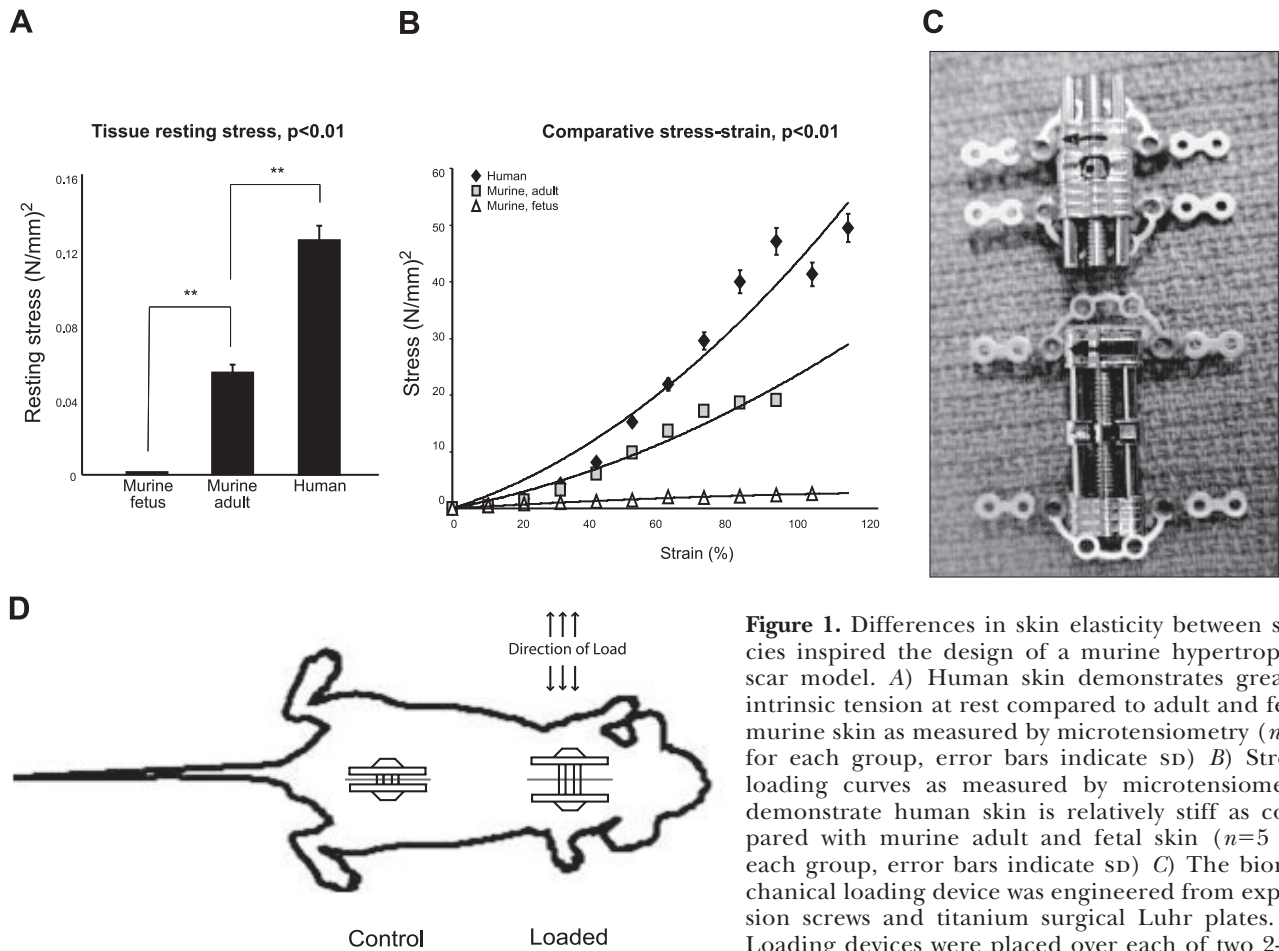


Figure 1. Differences in skin elasticity between species inspired the design of a murine hypertrophic scar model. *A*) Human skin demonstrates greater intrinsic tension at rest compared to adult and fetal murine skin as measured by microtensiometry ($n=5$ for each group, error bars indicate SD) *B*) Stress-loading curves as measured by microtensiometry demonstrate human skin is relatively stiff as compared with murine adult and fetal skin ($n=5$ for each group, error bars indicate SD) *C*) The biomechanical loading device was engineered from expansion screws and titanium surgical Luhr plates. *D*) Loading devices were placed over each of two 2-cm

linear incisions on the mouse dorsum. One wound was left unloaded and served as the internal control, while the other was subjected to mechanical loading and served as the experimental wound.

Hypertrophic scarring is independent of the direction of applied load

To eliminate the possibility that we were producing a gradual wound dehiscence or separation, we altered the vector of the mechanical force so that it was applied parallel to the wound. This vector orientation resulted in forces which brought the wound edges together while still delivering load to the surrounding skin and wound margin (Supplemental Fig. 2A). After such exposure to longitudinal mechanical loading, we again observed increased hyperplasia and fibrosis compared to control wounds (0.87 mm^2 vs. 0.18 mm^2 , $P<0.01$) (Supplemental Fig. 2B). With either parallel or perpendicular load, collagen was arranged in sheets parallel to the direction of applied load (data not shown). These studies confirm that mechanical loading, induced over a 7-day period, is necessary to generate human-like hypertrophic scar formation in mice.

Mechanical load-induced hypertrophic scars feature all of the classic histopathological characteristics of human hypertrophic scars

Although we observed that mechanical loading results in abnormal scar formation in mice, it was initially

unclear how closely this process resembled human scar formation. Excessive scarring in humans is either classified as hypertrophic scarring or keloid formation. Keloids are less common and are believed to be genetically influenced (6, 35), whereas hypertrophic scars can occur in any human wound and are the most common cause of functional disability related to scar contracture. The histological criteria used to differentiate hypertrophic scars from keloids and normal scars are summarized in **Table 1** (36–40).

Detailed histopathological comparison of our murine scars with human specimens revealed that they duplicated all of the features of human hypertrophic scars (**Fig. 2**) (37–39, 41, 42). Like human hypertrophic scars, the murine scars are raised (**Fig. 2A**) and showed epidermal thickening with adnexal structures and hair follicles absent in the dermis (**Fig. 2B**). Collagen was arranged in compact sheets parallel to the direction of applied load with fibroblasts aligning with the collagen fibers (**Fig. 2C**). Like human hypertrophic scars, mechanically induced scars showed a significant mast cell infiltrate (**Fig. 2D**). The mechanically loaded murine wounds also demonstrated hypervascularity (**Fig. 2E**), a classic feature of hypertrophic scars. Collagen whorls—often seen in mature human hypertrophic scars (37, 38, 42)—were also present in our murine model after 24

TABLE 1. *Histological similarities and differences between keloid, hypertrophic scar, and normal scar*

Scar Characteristics (37–42)	Hypertrophic Scar	Keloid	Normal Scar
Raised scar (Figure 2A).	Yes	Yes	Some
Loss of rete pegs, adnexae, and hair follicles (Figure 2B).	Yes	Yes	No
Fibrillary collagen and fibroblasts are arranged parallel to the skin surface (Figure 2C).	Yes	No	No
Increased mast cell density (Figure 2D).	Yes	No	No
Hypervascularity (Figure 2E).	Yes	No	No
Collagen whorls in scars (Figure 2F).	Yes	Yes	No
Increased number of fibroblasts (Figure 5B).	Yes	No	Some
Large thick collagen fibrils packed closely together	No	Yes	No
Scarring beyond wound margins	No	Yes	No

wk (Fig. 2F). Finally, cellular hyperplasia occurred in the loaded murine scars (Fig. 5B). The striking similarity to human hypertrophic scars suggested that this murine model would be useful to investigate the pathophysiology of human hypertrophic scarring.

Changes in scar morphology are permanent following a brief exposure to load

In all cases, the control wounds healed with almost no scarring at 2 wk (Fig. 3A, E), whereas the loaded regions had significantly increased volume and cellularity and resembled human hypertrophic scars (38, 41, 42) (Fig. 3B, C, D, F, G, H). To control for possible anatomic differences in scar morphology, we alternated activation of the cranial and caudal devices and observed no differences (data not shown).

After 2 wk of loading, mechanically induced scars showed dramatically increased thickness (Fig. 4A) and at least twenty-fold increases in cross sectional area (Fig. 4B). At later time points (wk 4 through 24), the loaded scars maintained their increased volume and thickness (Fig. 4A, B). Interestingly, collagen production per cell remained unchanged between control and mechanically induced scars through the 3 wk after initiation of distraction (Fig. 4C). By 3 wk, scar thickness and cross-sectional area had reached maximal levels, leading us to conclude that the dramatically increased collagen deposition during this early time period was likely due to increased cellularity, not to increased collagen production per cell.

Increased cellularity is a constant feature of hypertrophic scars and is due to decreased cellular apoptosis in vivo

The cellular density per square millimeter was consistently higher in loaded scars (Fig. 5B, C) than in control scars (Fig. 5A), another feature of human hypertrophic scars. This difference was observed at all time points (Fig. 5D, E).

Potential etiologies for increased cellular density are increased cellular proliferation or decreased cellular apoptosis. Using BRDU immunohistochemistry, we observed no significant differences in proliferation be-

tween the control (Fig. 6A) and loaded wounds (Fig. 6B). Quantifying these differences, we confirmed that cellular proliferation was unchanged by applying mechanical stress to healing wounds over time (Fig. 6C). In contrast, cellular apoptosis was significantly decreased during the early phases of wound healing in the loaded scars as compared to the controls as determined by cleaved caspase-3 immunohistochemistry ($P < 0.05$) (Fig. 6D).

Western blots of wound homogenates confirmed 10-fold less expression of the late downstream proapoptotic marker cleaved caspase-3 in mechanically loaded wounds compared with control wounds at 2 wk ($P < 0.05$) (Fig. 6E). An obvious candidate for upstream apoptosis signaling is the PI3-kinase/Akt pathway, known to be activated by actin stabilization and FAK up-regulation and thought to be mechanically induced (22). In our model, wound homogenates showed significantly increased activated p-Akt protein in the mechanically loaded wounds compared with controls at 1 wk (Fig. 6F).

Altered Akt-dependent apoptosis pathways affect scar hypertrophy in knockout mice

To confirm the importance of stress-induced decreases in fibroblast apoptosis, we examined whether blocking apoptotic pathways would change hypertrophic scar formation. The proapoptotic regulator p53 and anti-apoptotic regulator *BclII*, both Akt-dependent, were specifically examined. As predicted, loaded wounds from p53 null mice showed significantly higher cross-sectional area (5.7 mm^2 vs. 2.5 mm^2 , $P < 0.01$) (Fig. 7A, top) and greater gross scar hypertrophy (Fig. 7D, top) when compared to wild-type mice (Fig. 7B, E, top). In contrast, loaded wounds from *BclII* null mice showed significantly less cross-sectional area (0.64 mm^2 , $P < 0.001$) (Fig. 7C, top) and almost no gross scar hypertrophy (Fig. 7F, top) when compared to wild-type mice (Fig. 7B, E, top). Quantification of scar area confirmed these differences (Fig. 7G). These differences are maintained through 24 wk following initiation of distraction (Fig. 7I).

Significantly, the control scars in the p53 null (Fig. 7A, bottom), wild-type (Fig. 7B, bottom), and *BclII* null (Fig. 7C, bottom) mice were almost identical with respect

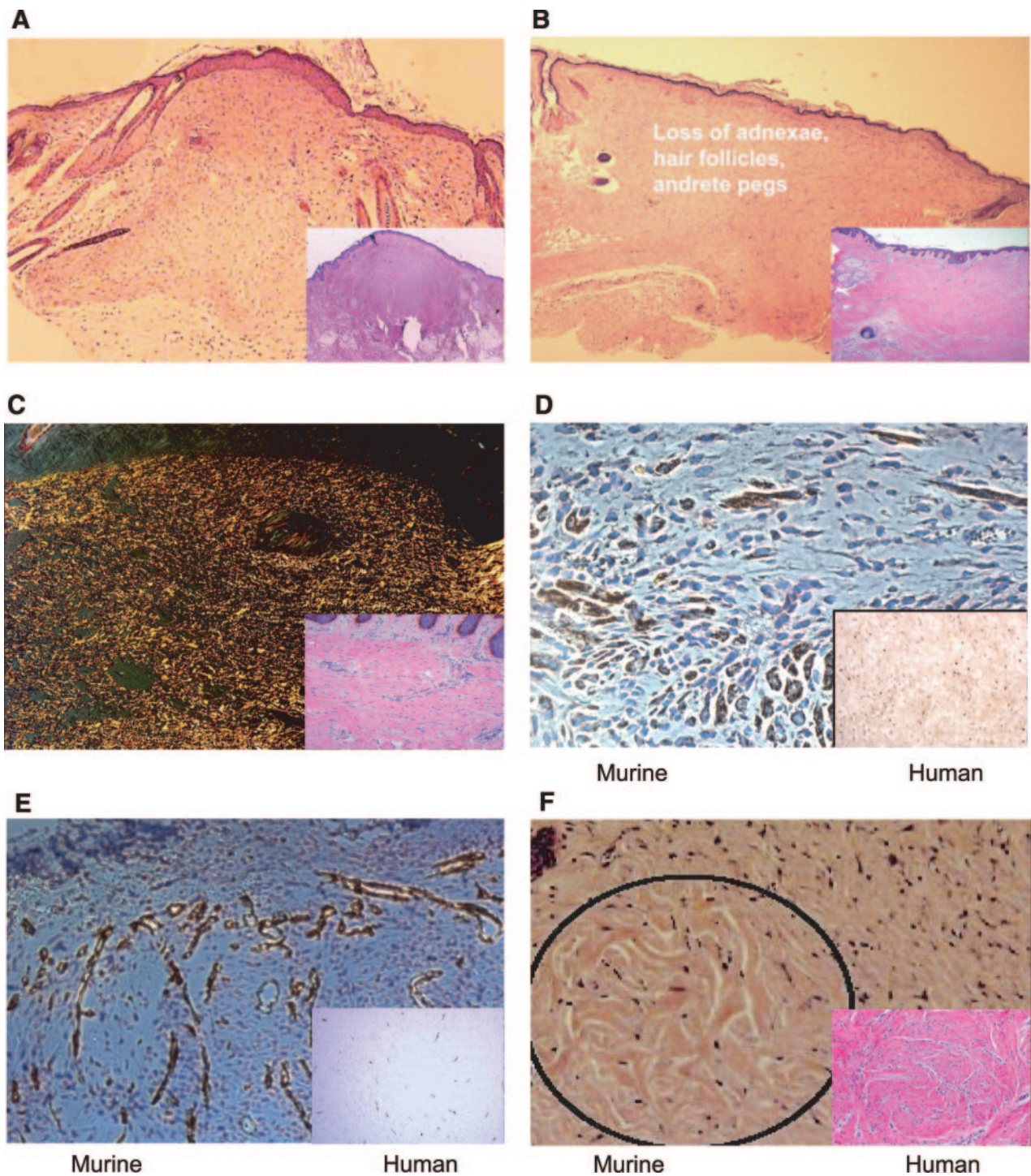


Figure 2. Murine loaded scars at 2 wk demonstrate all the classic histological features of human hypertrophic scars (*inset*). *A*) At 2 wk, murine loaded scars are raised and *B*) demonstrate a loss of rete pegs, adnexae, and hair follicles. *C*) Also at 2 wk, fibroblasts are oriented parallel to the sheet-like collagen fibers and to the direction of loading and show *D*) increased mast cell density, as demonstrated by CD117 immunohistochemistry. *E*) CD31 (an endothelial marker) immunostaining demonstrates hypervascularity in loaded wounds after 2 wk. *F*) Collagen whorls, seen in mature human hypertrophic scars, are also seen in loaded murine scars after 24 wk.

to total cross-sectional area. Grossly, the p53 null (Fig. 7D, *bottom*), wild-type (Fig. 7E, *bottom*), and *BclII* null (Fig. 7F, *bottom*) control scars were indistinguishable from one another. There was no difference in quantified scar areas between the three control groups (Fig. 7H). These data, taken together, dem-

onstrate that decreased apoptotic pathways resulting in hypertrophic scar formation are only present following timed mechanical loading. Interestingly, there was no significant difference in breaking strengths of the loaded wounds among the three groups (data not shown).

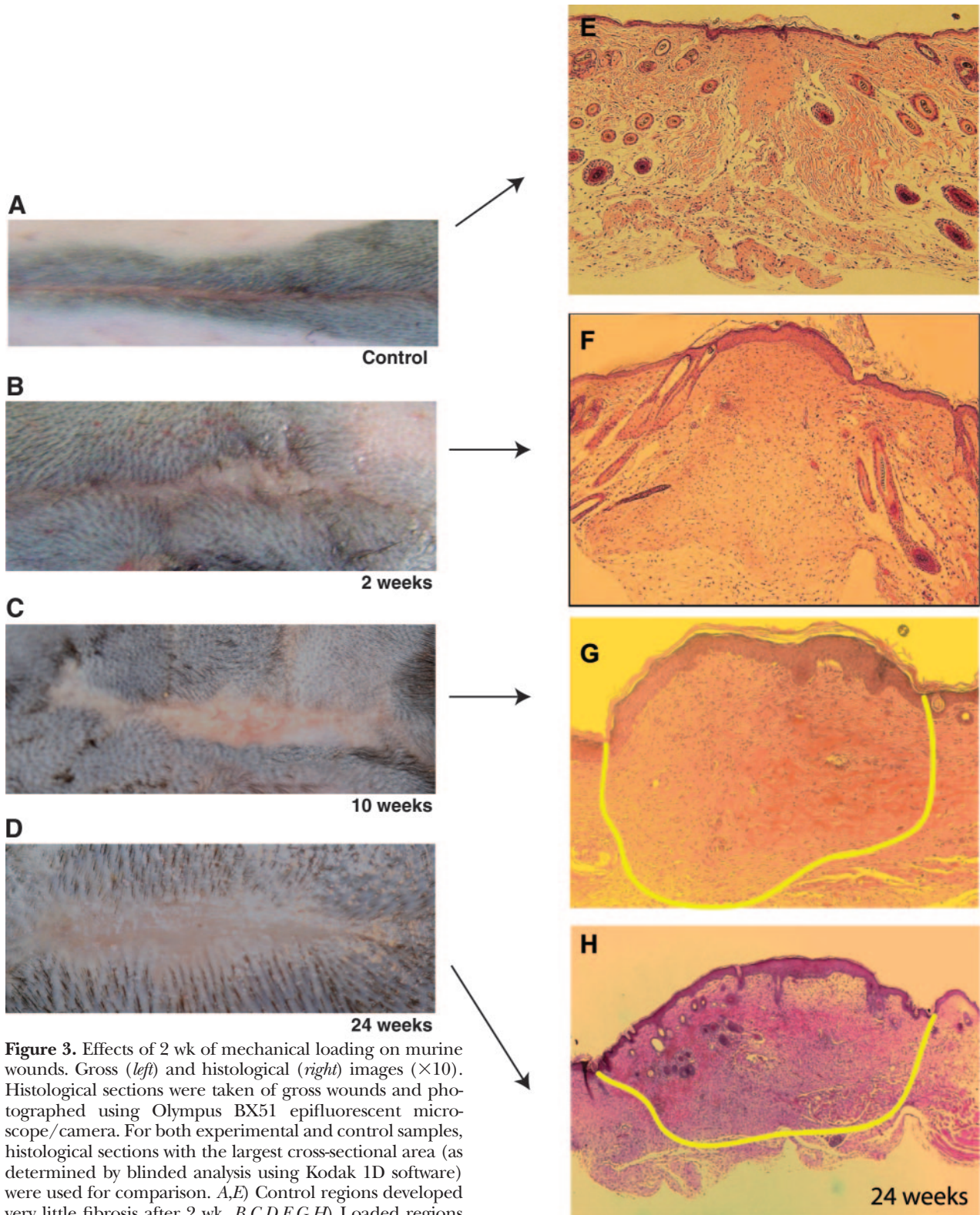


Figure 3. Effects of 2 wk of mechanical loading on murine wounds. Gross (*left*) and histological (*right*) images ($\times 10$). Histological sections were taken of gross wounds and photographed using Olympus BX51 epifluorescent microscope/camera. For both experimental and control samples, histological sections with the largest cross-sectional area (as determined by blinded analysis using Kodak 1D software) were used for comparison. *A,E*) Control regions developed very little fibrosis after 2 wk. *B,C,D,F,G,H*) Loaded regions developed into hypertrophic scars with 20-fold greater cross-sectional area than control regions.

DISCUSSION

Current therapies for hypertrophic scarring are ineffective because of limited understanding into the pathogenesis of the underlying fibroproliferative process.

Prior research has contributed fragments of insight into the disease process but has been largely descriptive because of the lack of an appropriate animal model. Animal models currently in use, such as the rabbit ear or Red Duroc pig, are in species for which many

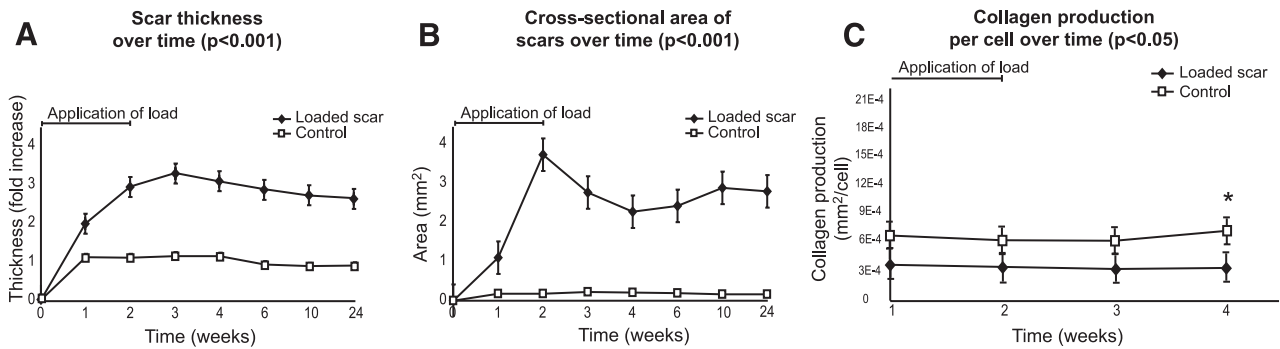


Figure 4. Loaded murine scars maintain increased area and thickness over time. *A*) After 2 wk of loading, mechanically induced scars showed dramatically increased thickness, which was maintained through 24 wk. *B*) Analysis of scar histology by Kodak 1D software shows scar area in loaded regions was almost 20-fold greater than in control regions even after 24 wk (3.78 mm² vs. 0.18 mm² at week 2; 2.3 mm² vs. 0.21 mm² at week 4; 2.83 mm² vs. 0.17 mm² at 6 months) ($n=5$ for each group, error bars indicate SD). *C*) Collagen production per cell remained unchanged between control and mechanically induced scars through 3 wk after initiation of distraction. Since at 3 wk, scar thickness and cross-sectional area had reached maximal levels, we concluded that the dramatically increased collagen deposition during this early time period was likely due to increased cellularity, not to increased collagen production per cell.

molecular biology techniques are not available. While some insights into the pathogenesis of fibroproliferative disease have been gained, these models do not reproduce the factors thought to initiate the human disease. In this manuscript, we describe the first murine model of hypertrophic scarring, produced by applying exogenous mechanical forces onto healing murine wounds. This was accomplished using a novel tension device that augments the physiologically low levels of resting tension on murine skin to levels experienced by normal human skin. When applied early in wound healing, this results in healed scars that are grossly and histologically identical to human hypertrophic scars.

Our experiments implicate the Akt pathway in fibroblasts as a key effector of hypertrophic scar formation

by inhibiting apoptosis and leading to an accumulation of fibroblasts in the healing wound. It is well established that Akt acts as a proto-oncogene promoting cell survival (43). It has previously been shown that on the fibroblast surface, cytoskeletal interactions with integrins and signaling to focal adhesion kinases act to phosphorylate and activate Akt in fibroblasts. This suggests that mechanical stress may activate multiple prosurvival pathways in fibroblasts, leading to a robust accumulation of cells in healing wounds.

Akt acts to phosphorylate Bad, a negative regulator of bcl-2, thereby inactivating it. This removes inhibition of bcl-2, which, in turn, down-regulates apoptosomal activation by bax and bak and inhibits apoptosis. Further, Akt also decreases apoptosis by directly up-regulating

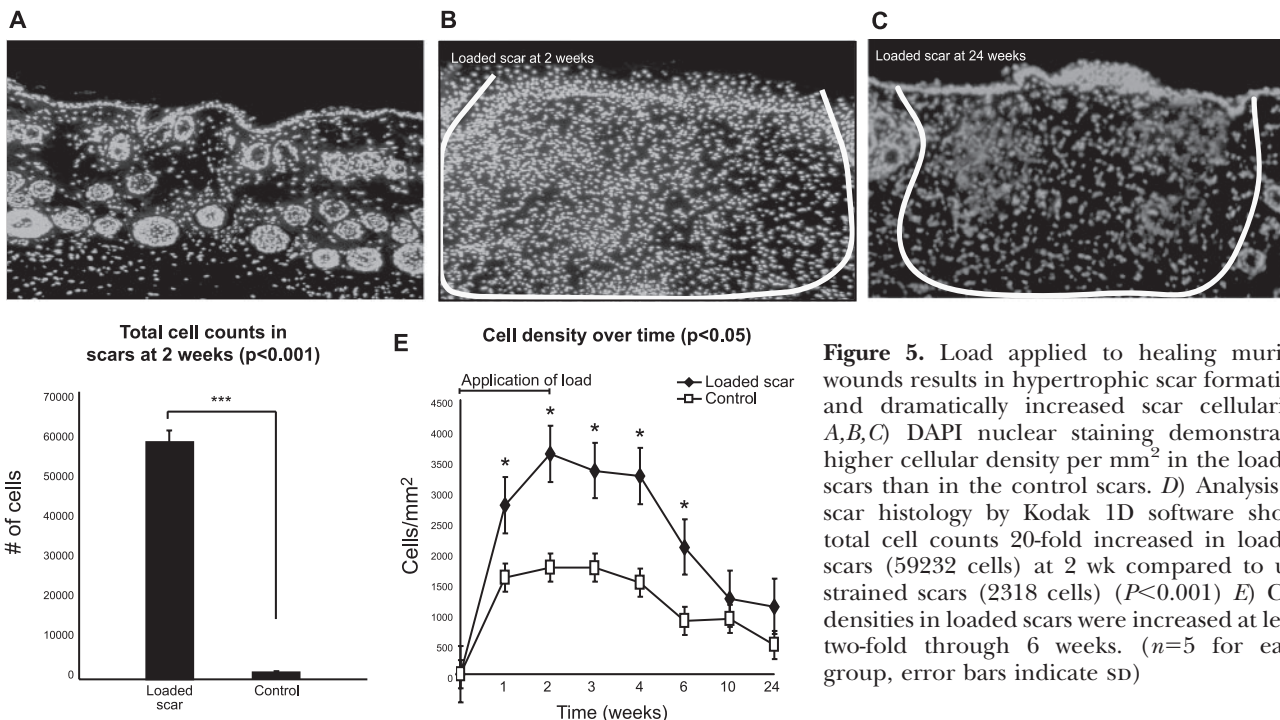


Figure 5. Load applied to healing murine wounds results in hypertrophic scar formation and dramatically increased scar cellularity. *A, B, C*) DAPI nuclear staining demonstrates higher cellular density per mm² in the loaded scars than in the control scars. *D*) Analysis of scar histology by Kodak 1D software shows total cell counts 20-fold increased in loaded scars (59232 cells) at 2 wk compared to unstrained scars (2318 cells) ($P < 0.001$) *E*) Cell densities in loaded scars were increased at least two-fold through 6 weeks. ($n=5$ for each group, error bars indicate SD)

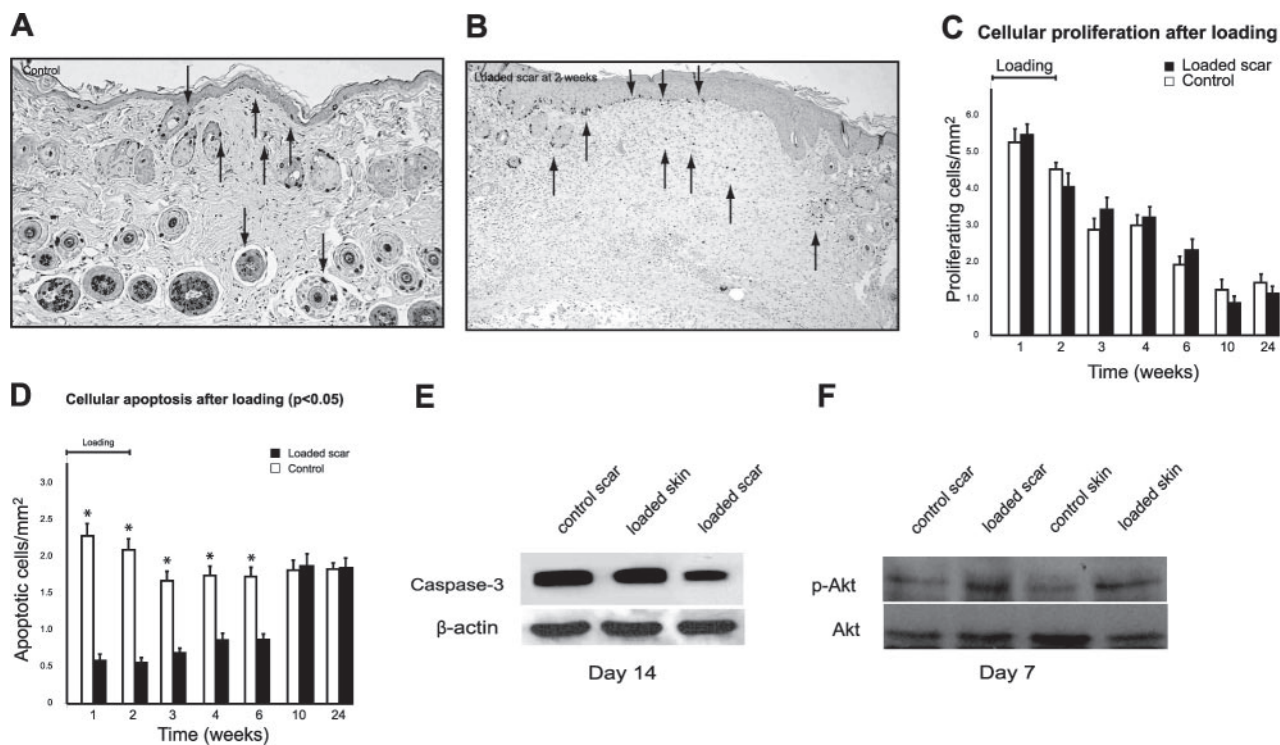


Figure 6. Hypertrophic scar formation is due to decreased Akt-dependent cellular apoptosis. *A,B*) BRDU staining demonstrates proliferating cells in the epidermis (arrows) and hair follicles in both control and loaded wounds. *C*) Cell counts of BRDU+ cells/hpf show no significant difference in cellular proliferation between the loaded and control regions. *D*) Cleaved-caspase 3 antibody expression in tissue sections is significantly less in loaded scars through 6 wk ($P<0.05$). *E*) Cleaved-caspase 3 protein level, as determined by Western blot is 10-fold less in loaded wounds (0.2 relative band intensity to control nonwounded skin) than in control wounds (1.97 relative band intensity) after 2 wk ($P<0.05$). *F*) Akt protein activation (p-Akt) is dramatically increased in loaded wounds compared with control wounds at 1 wk. For data presented in all panels, $n = 5$ for each group, error bars indicate sd.

cyclic AMP-related binding protein (CREB), which also increases *BclII* (44). Thus, in the *BclII* null mice, the absence of functional *BclII* blocks the protective effects of the Akt pathway (45) and results in increased fibroblast apoptosis. This manifests as an inability to form hypertrophic scars in our experimental model.

In contrast, Akt inhibits p53-mediated apoptosis via direct and indirect mechanisms. Up-regulation of Akt leads to Mdm2 stimulation and inactivation of p53-related apoptosis (46). In p53 null mice, the effects of stress-induced up-regulation of Akt leads to decreased apoptosis, increased cellular accumulation, and dramatic hypertrophic scar formation. These data correlate with previous work showing that mechanical stress acts to inhibit fibroblast apoptosis (47, 48). Taken together, these results suggest targeted intervention to uncouple mechanical signaling or to uncouple Akt and downstream apoptotic pathways would be useful therapeutic strategies to eliminate hypertrophic scar formation.

It seems likely that the mechanoresponsive properties of fibroblasts have an evolutionarily conserved function. After disruption of the skin, cells along wound edges are exposed to high levels of stress leading to activated mechanical signaling and a pro-survival environment for cells in the healing wound. However, as wound healing proceeds, the deposited

matrix reestablishes a homogenous mechanical environment, turning off these signals and allowing programmed cell death to occur. In the process of hypertrophic scar formation, high levels of local wound stress prevent this transition and create a prolongation of the antiapoptotic milieu characteristic of the healing wound. Thus, the development of asymmetric gradients of stress and their eventual restoration to homeostasis may be important and unsuspected signaling events in the wound healing cascade.

It is possible that these same processes underlie commonly observed differences in skin architecture seen within the same organism at different stages in embryogenesis or at different anatomic locations. During development, changing body size results in altered mechanical forces on the skin of an organism. Cells exposed to these stresses may have enhanced survival and increased production of damping matrix components. Thus, areas of the body subjected to highest stress, such as appendicular joints or the feet, would remodel to increase dermal thickness by increasing cellularity and subsequent matrix production. We believe that a similar linear and proportional mechanosensing response occurs following wounding. During hypertrophic scar formation, the physiological mechanosensing response becomes pathologically activated. With modern surgical advances and the use of sutures,

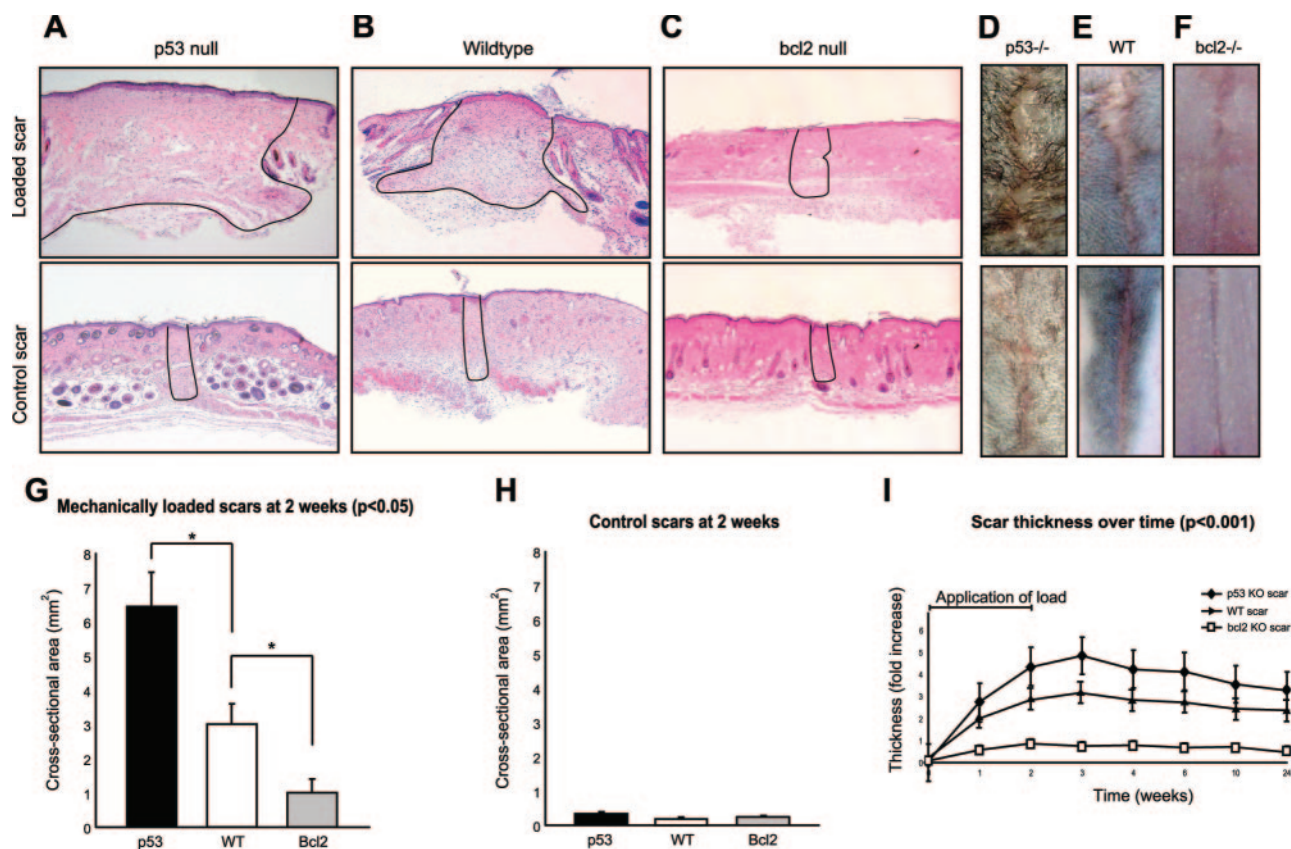


Figure 7. Effects of mechanical loading on antiapoptotic (p53) and proapoptotic (*BclII*) knockout mice. Images are of 2-wk scars. (A,B,C, Top) There was a marked difference in the scar area in antiapoptotic p53^{-/-} (5.7 mm²) and proapoptotic *BclII*^{-/-} (0.64 mm²) mice under loading, as compared to wild-type controls (2.5 mm², $P < 0.001$). (A,B,C, Bottom) In contrast, no differences were observed among the three groups in the absence of loading. (D,E,F, Top) This was also obvious on gross examination with loaded scars averaging 3 mm of height above the skin surface. (D,E,F, Bottom) Control scars remained flat. G) Quantifying the cross-sectional areas of the loaded wounds confirmed significant differences among control, p53 null, and *BclII* null scars ($P < 0.05$). H) There were no differences among the three groups in the absence of loading. I) These differences in scar thickness were maintained through 24 wk ($P < 0.001$). For data presented in all panels, $n = 5$ for each group, error bars indicate SD.

the protective effect humans may have derived from hypertrophic scarring is vestigial and dysfunctional, leading to significant human morbidity in the form of joint contractures and disfigurement.

The phenotypic changes we observed in response to mechanical stress were independent of the vector of force applied. Furthermore, brief periods of human-level stress were sufficient for excessive wound fibrosis to persist permanently. Hypertrophic scar development did not occur if stress were applied outside of this critical time window. The nature of this time-dependence is an area of active investigation and may further offer fundamental insights into the wound healing. It is interesting that this vulnerable window for hypertrophic scar formation coincides with the period during which monocytes and macrophages become the predominant cell type within the healing wound.

There is a sizeable body of literature suggesting the importance of the inflammatory process in stimulating fibrosis. The interplay of inflammatory cells with fibroblasts is well documented (49), and it is likely that as mechanical stress leads to fibroblast accumulation, soluble mediators such as TGF β , PDGF, and FGF act as chemoattractants and stimulate matrix production by

these stromal cells (2, 50). This positive feedback would maximize fibrosis during wound healing and lead to hypertrophic scarring. Whether inflammatory cells are themselves mechanoresponsive and exactly how exactly the fibroblast synthetic phenotype is altered by inflammatory cells is an area of active investigation. As stimulated fibroblasts lay an abundant collagen matrix, a number of other fibroblast-derived factors such as plasminogen and collagenases are active in remodeling the fibrotic mass of scar tissue, a process that can last months to years (2, 50).

Traditional therapeutics for hypertrophic scarring exert their effects by inhibiting inflammation (*e.g.*, radiation and steroids) or by reducing the mechanical stimuli that lead to hypertrophic scarring (*e.g.*, pressure garments). Unfortunately, these approaches also interfere with physiologically necessary components of wound healing (*i.e.*, inflammation and neovascularization) and are not sufficiently selective to target the cellular events that lead to the disease. In this manuscript, we have demonstrated that by shifting the balance of apoptosis using molecular strategies, we can dramatically impact subsequent hypertrophic scar formation. This suggests that targeting apoptosis and its

upstream activators may be therapeutically useful, especially since this does not appear to compromise the ultimate strength of the healing wound. Topical applications to induce Akt-dependent fibroblast apoptosis seem promising for reducing scar formation, particularly early in the proliferative phase of wound healing. Once specific mediators of the mechanotransduction cascade are better understood (i.e., integrins, FAK, etc.), these may also be candidates for targeted therapy. Directly modulating the gross mechanical forces acting on the healing wound may be an alternative to molecular therapy, although it is not clear whether this will be technically feasible.

It seems paradoxical that wounds healing with less matrix deposition are as strong as those healing with abundant matrix. Most likely, hypertrophic scarring represents the extreme phenotype of the normal physiological response to mechanical tension. That is, it is possible that the extra matrix present in the process of hypertrophic scar formation is too rapidly and abundantly deposited to be amenable to remodeling and reorganization, which are critical events for scar strengthening. Thus, the resulting excessive and disorganized matrix may not contribute to overall scar strength. Currently, most attempts at treatment begin late in course of the disease, at a time our data suggest the process of hypertrophic scarring is already well established. As previously discussed, our results seem to indicate a discrete window early in the proliferative phase of wound healing, during which mechanical stress maximally activates the process of hypertrophic scarring. Our data suggest that early, specifically targeted treatment—before any external manifestation of the disease is present—may provide the best opportunity toward halting the disease process.

The importance of similar mechanical signaling pathways in the pathogenesis of other human diseases remains unclear. Experimentally, distraction osteogenesis and models of hypertension have mechanically induced tissue growth. Further, diseases in which altered mechanical conditions correlate with increased tissue fibrosis and hypertrophy affect almost every organ system. Pulmonary fibrosis (51), congestive heart failure (52, 53), and glomerulosclerosis (24) are among the diseases in which increased levels of mechanical loading correlate with the development of fibroproliferative disease. Traditionally, the focus of treatment in these diseases has been to reverse aberrant macroscopic forces that produce a gross distortion of tissue architecture through volume, flow, and pressure changes. Here, we demonstrate that focusing on the cellular and intracellular consequences of the mechanical environment may also be a useful strategy to identify new therapeutic approaches for fibroproliferative diseases of the skin and other organ systems. FJ

This work was funded in part by the National Institutes of Health through the following grants: R01 NIA AG-021494 (G.C. Gurtner), R01 NID DK067771 (G. C. Gurtner), R01 HL-075639 (J. Holmes), AHA 0525962T (S.A. Loh).

REFERENCES

- Martin, P. (1997) Wound healing—aiming for perfect skin regeneration. *Science* **276**, 75–81
- Singer, A. J., and Clark, R. A. (1999) Cutaneous wound healing. *N. Engl. J. Med.* **341**, 738–746
- Singer, A. J., Hollander, J. E., and Quinn, J. V. (1997) Evaluation and management of traumatic lacerations. *N. Engl. J. Med.* **337**, 1142–1148
- Wilson, I. F., Lokeh, A., Schubert, W., and Benjamin, C. I. (2000) Latissimus dorsi myocutaneous flap reconstruction of neck and axillary burn contractures. *Plast. Reconstr. Surg.* **105**, 27–33
- Sheridan, R. L. (2000) Airway management and respiratory care of the burn patient. *Int. Anesthesiol. Clin.* **38**, 129–145
- Deitch, E. A., Wheelahan, T. M., Rose, M. P., Clothier, J., and Cotter, J. (1983) Hypertrophic burn scars: analysis of variables. *J. Trauma.* **23**, 895–898
- Mustoe, T. A., Cooter, R. D., Gold, M. H., Hobbs, F. D., Ramelet, A. A., Shakespeare, P. G., Stella, M., Teot, L., Wood, F. M., and Ziegler, U. E. (2002) International clinical recommendations on scar management. *Plast. Reconstr. Surg.* **110**, 560–571
- Sheridan, R. L., and Tompkins, R. G. (2004) What's new in burns and metabolism. *J. Am. Coll. Surg.* **198**, 243–263
- Suzuki, S., Matsuda, K., and Nishimura, Y. (1996) Proposal for a new comprehensive classification of V-Y plasty and its analogues: the pros and cons of inverted versus ordinary Burrow's triangle excision. *Plast. Reconstr. Surg.* **98**, 1016–1022
- Longacre, J. J., Berry, H. K., Basom, C. R., and Townsend, S. F. (1976) The effects of Z plasty on hypertrophic scars. *Scand. J. Plast. Reconstr. Surg.* **10**, 113–128
- Burke, M. (1998) Scars. Can they be minimised? *Aust. Fam. Physician.* **27**, 275–278
- Edlich, R. F., and Carl, B. A. (1998) Predicting scar formation: from ritual practice (Langer's lines) to scientific discipline (static and dynamic skin tensions). *J. Emerg. Med.* **16**, 759–760
- Suzuki, S., Um, S. C., Kim, B. M., Shin-ya, K., Kawai, K., and Nishimura, Y. (1998) Versatility of modified planimetric Z-plasties in the treatment of scar with contracture. *Br. J. Plast. Surg.* **51**, 363–369
- Robson, M. C., Barnett, R. A., Leitch, I. O., and Hayward, P. G. (1992) Prevention and treatment of postburn scars and contracture. *World J. Surg.* **16**, 87–96
- Sherris, D. A., Larrabee, W. F., Jr., and Murakami, C. S. (1995) Management of scar contractures, hypertrophic scars, and keloids. *Otolaryngol. Clin. North Am.* **28**, 1057–1068
- Costa, A. M., Peyrol, S., Porto, L. C., Comparin, J. P., Foyatier, J. L., and Desmouliere, A. (1999) Mechanical forces induce scar remodeling. Study in non-pressure-treated versus pressure-treated hypertrophic scars. *Am. J. Pathol.* **155**, 1671–1679
- Reno, F., Sabbatini, M., Lombardi, F., Stella, M., Pezzuto, C., Magliacani, G., and Cannas, M. (2003) In vitro mechanical compression induces apoptosis and regulates cytokines release in hypertrophic scars. *Wound Repair Regen.* **11**, 331–336
- Bao, G., and Suresh, S. (2003) Cell and molecular mechanics of biological materials. *Nat. Mater.* **2**, 715–725
- Alenghat, F. J., and Ingber, D. E. (2002) Mechanotransduction: all signals point to cytoskeleton, matrix, and integrins (Online). *Sci. STKE* **2002**, PE6
- Hynes, R. O. (1992) Integrins: versatility, modulation, and signaling in cell adhesion. *Cell* **69**, 11–25
- Schaller, M. D., Borgman, C. A., Cobb, B. S., Vines, R. R., Reynolds, A. B., and Parsons, J. T. (1992) pp125FAK a structurally distinctive protein-tyrosine kinase associated with focal adhesions. *Proc. Natl. Acad. Sci. U. S. A.* **89**, 5192–5196
- Miranti, C. K., and Brugge, J. S. (2002) Sensing the environment: a historical perspective on integrin signal transduction. *Nat. Cell Biol.* **4**, E83–E90
- Sugden, P. H. (2003) Ras, Akt, and mechanotransduction in the cardiac myocyte. *Circ. Res.* **93**, 1179–1192
- Riser, B. L., Varani, J., Cortes, P., Yee, J., Dame, M., and Sharba, A. K. (2001) Cyclic stretching of mesangial cells up-regulates intercellular adhesion molecule-1 and leukocyte adherence: a possible new mechanism for glomerulosclerosis. *Am. J. Pathol.* **158**, 11–17

25. Ingber, D. E. (2003) Mechanobiology and diseases of mechanotransduction. *Ann. Med.* **35**, 564–577
26. Wang, J., Zohar, R., and McCulloch, C. A. (2006) Multiple roles of alpha-smooth muscle actin in mechanotransduction. *Exp. Cell Res.* **312**, 205–214
27. Wang, Z., Fong, K. D., Phan, T. T., Lim, I. J., Longaker, M. T., and Yang, G. P. (2006) Increased transcriptional response to mechanical strain in keloid fibroblasts due to increased focal adhesion complex formation. *J. Cell Physiol.* **206**, 510–517
28. Gabbiani, G. (2003) The myofibroblast in wound healing and fibrocontractive diseases. *J. Pathol.* **200**, 500–503
29. Greenhalgh, D. G. (1998) The role of apoptosis in wound healing. *Int. J. Biochem. Cell Biol.* **30**, 1019–1030
30. Qian, Y., Zhong, X., Flynn, D. C., Zheng, J. Z., Qiao, M., Wu, C., Dedhar, S., Shi, X., and Jiang, B. H. (2005) ILK mediates actin filament rearrangements and cell migration and invasion through PI3K/Akt/Rac1 signaling. *Oncogene* **24**, 3154–3165
31. Umeda, J., Sano, S., Kogawa, K., Motoyama, N., Yoshikawa, K., Itami, S., Kondoh, G., Watanabe, T., and Takeda, J. (2003) In vivo cooperation between Bcl-xL and the phosphoinositide 3-kinase-Akt signaling pathway for the protection of epidermal keratinocytes from apoptosis. *FASEB J.* **17**, 610–620
32. Martin, P., and Parkhurst, S. M. (2004) Parallels between tissue repair and embryo morphogenesis. *Development* **131**, 3021–3034
33. Colwell, A. S., Longaker, M. T., and Lorenz, H. P. (2003) Fetal wound healing. *Front. Biosci.* **8**, S1240–S1248
34. Clark, J. A., Cheng, J. C., and Leung, K. S. (1996) Mechanical properties of normal skin and hypertrophic scars. *Burns* **22**, 443–446
35. Marneros, A. G., Norris, J. E., Watanabe, S., Reichenberger, E., and Olsen, B. R. (2004) Genome scans provide evidence for keloid susceptibility loci on chromosomes 2q23 and 7p11. *J. Invest. Dermatol.* **122**, 1126–1132
36. Brissett, A. E., and Sherris, D. A. (2001) Scar contractures, hypertrophic scars, and keloids. *Facial Plast. Surg.* **17**, 263–272
37. Santucci, M., Borgognoni, L., Reali, U. M., and Gabbiani, G. (2001) Keloids and hypertrophic scars of Caucasians show distinctive morphologic and immunophenotypic profiles. *Virchows. Arch.* **438**, 457–463
38. Ehrlich, H. P., Desmouliere, A., Diegelmann, R. F., Cohen, I. K., Compton, C. C., Garner, W. L., Kapanci, Y., and Gabbiani, G. (1994) Morphological and immunochemical differences between keloid and hypertrophic scar. *Am. J. Pathol.* **145**, 105–113
39. Lee, J. Y., Yang, C. C., Chao, S. C., and Wong, T. W. (2004) Histopathological differential diagnosis of keloid and hypertrophic scar. *Am. J. Dermatopathol.* **26**, 379–384
40. Tuan, T. L., and Nichter, L. S. (1998) The molecular basis of keloid and hypertrophic scar formation. *Mol. Med. Today* **4**, 19–24
41. White, C. R. (2004) *Textbook of Dermatopathology*, McGraw Hill, New York
42. Linares, H. A., Kischer, C. W., Dobrkovsky, M., and Larson, D. L. (1972) The histiotypic organization of the hypertrophic scar in humans. *J. Invest. Dermatol.* **59**, 323–331
43. Amaravadi, R., and Thompson, C. B. (2005) The survival kinases Akt and Pim as potential pharmacological targets. *J. Clin. Invest.* **115**, 2618–2624
44. Pugazhenth, S., Nesterova, A., Sable, C., Heidenreich, K. A., Boxer, L. M., Heasley, L. E., and Reusch, J. E. (2000) Akt/protein kinase B up-regulates Bcl-2 expression through cAMP-response element-binding protein. *J. Biol. Chem.* **275**, 10761–10766
45. Flusberg, D. A., Numaguchi, Y., and Ingber, D. E. (2001) Cooperative control of Akt phosphorylation, bcl-2 expression, and apoptosis by cytoskeletal microfilaments and microtubules in capillary endothelial cells. *Mol. Biol. Cell* **12**, 3087–3094
46. Gottlieb, T. M., Leal, J. F., Seger, R., Taya, Y., and Oren, M. (2002) Cross-talk between Akt, p53 and Mdm2: possible implications for the regulation of apoptosis. *Oncogene* **21**, 1299–1303
47. Linge, C., Richardson, J., Vigor, C., Clayton, E., Hardas, B., and Rolfe, K. (2005) Hypertrophic scar cells fail to undergo a form of apoptosis specific to contractile collagen—the role of tissue transglutaminase. *J. Invest. Dermatol.* **125**, 72–82
48. Varedi, M., Tredget, E. E., Ghahary, A., and Scott, P. G. (2000) Stress-relaxation and contraction of a collagen matrix induces expression of TGF-beta and triggers apoptosis in dermal fibroblasts. *Biochem. Cell Biol.* **78**, 427–436
49. Wynn, T. A. (2004) Fibrotic disease and the T(H)1/T(H)2 paradigm. *Nat. Rev. Immunol.* **4**, 583–594
50. Sheridan, R. L. (2003) Burn care: results of technical and organizational progress. *JAMA* **290**, 719–722
51. Vittal, R., Horowitz, J. C., Moore, B. B., Zhang, H., Martinez, F. J., Toews, G. B., Standiford, T. J., and Thannickal, V. J. (2005) Modulation of prosurvival signaling in fibroblasts by a protein kinase inhibitor protects against fibrotic tissue injury. *Am. J. Pathol.* **166**, 367–375
52. Borer, J. S., Truter, S., Herrold, E. M., Falcone, D. J., Pena, M., Carter, J. N., Dumlaio, T. F., Lee, J. A., and Supino, P. G. (2002) Myocardial fibrosis in chronic aortic regurgitation: molecular and cellular responses to volume overload. *Circulation* **105**, 1837–1842
53. Zhang, S., Weinheimer, C., Courtois, M., Kovacs, A., Zhang, C. E., Cheng, A. M., Wang, Y., and Muslin, A. J. (2003) The role of the Grb2-p38 MAPK signaling pathway in cardiac hypertrophy and fibrosis. *J. Clin. Invest.* **111**, 833–841

Received for publication January 28, 2007.

Accepted for publication April 19, 2007.